Published in "The Journal of Physical Chemistry A 114(25): 6787–6794 , 2010"
which should be cited to refer to this work.

Radicals and Radical Ions Derived from Indole, Indole-3-carbinol and Diindolylmethane

Anna Błoch-Mechkour and Thomas Bally*

Department of Chemistry, University of Fribourg, CH-1700 Fribourg, Switzerland

Adam Sikora, Radosław Michalski, Andrzej Marcinek,* and Jerzy Gębicki

Institute of Applied Radiation Chemistry, Technical University, 90-924 Lodz, Poland

Received: December 23, 2009; Revised Manuscript Received: April 12, 2010

The primary products, i.e., the radical cations and radicals obtained on oxidation of the glucobrassicin metabolites (and dietary supplements), indole-3-carbinol (**I3C**) and diindolylmethane **(DIM**), and those from parent indole (**I**) are characterized in an ionic liquid and in Ar matrices. The radical cations of **I** and **I3C** are stable toward (photo)deprotonation under these conditions, but the resulting radicals can be generated by UV-photolysis of the neutral precursors. Two types of radicals, obtained by loss of hydrogen from N- and C-atoms, respectively, are found for **I3C** and **DIM**.

Introduction

A number of commonly consumed cruciferous vegetables such as broccoli, Brussels sprouts, and cabbage, are sources of glucobrassicin, a thioglucoside that is cleaved by the enzyme myrosinase, which is released from the same plants on chopping or chewing, to form an isothiocyanate.[1,2] On hydrolysis this compound releases thiocyanate to yield indole-3-carbinol (**I3C**). Under acidic conditions, **I3C** forms an indolynium cation[3] that in turn attacks **I3C**, under release of formaldehyde,[4] to form several oligomers, the most prominent of which is diindolylmethane (**DIM**, see Scheme 1).

Numerous studies have pointed toward immune supporting, cancer preventing, and antiandrogenic properties of these two compounds, in particular the more stable **DIM**,[5] although insufficient conclusive data seem to be available to justify the widespread use of these compounds as dietary supplements (the National Cancer Institute has engaged in a campaign of clinical trials to assess the medical usefulness of **I3C** and **DIM**[6]).

Because these compounds are easily oxidized, research on their biological mode of action has focused on their antioxidant properties. In this perspective, **I3C** has been studied by chemical and electrochemical oxidation methods.[7] However, in spite of the fact that much research has been done on the redox and acid−base properties of other indolyl radicals,[8−10] there is practically no information on the transient products of the oxidation of **I3C** and **DIM**, such as radical cations or radicals. We have therefore decided to explore these reactive intermediates and to study their properties.

To this end, we subjected **I3C** and **DIM** to oxidation under various conditions where the primary or secondary products can be observed, either as transients or under stable conditions. To identify possible radicals that may form as secondary products, we also subjected the two compounds to UV-photolysis. In order to establish in what way the carbinol or indolyl substituents influence the outcome of the experiments, we subjected parent indole to the same conditions. Finally, we resorted to different types of quantum chemical calculations to assign the spectra we obtained in our experiments and to understand the observed chemistry.

* To whom correspondence should be addressed.

Experimental and Computational Methods

Compounds. The ionic liquid, 1-butyl-3-methylimidazolium hexafluorophosphate ($BMIM^+PF_6^-$),[11] and urorosein[12] were synthesized according to literature procedures.

Other chemicals were commercially available from Sigma-Aldrich. All aqueous solutions were prepared using water purified by a Millipore Milli-Q system.

Matrix Isolation and Spectroscopy.[13] As the volatility of indole is insufficient to premix it with the host gas at room temperature, ground crystals were placed in a U-tube attached to the inlet system of the cryostat and held at −15 °C while a 9:1 mixture of argon and nitrogen (which is added to improve the optical quality of matrices) was flowed through the U-tube and slowly deposited on a CsI window maintained at ca. 20 K.

The even lower volatilty of **I3C** necessitated the use of a sublimation oven, a double-walled glass tube fitted to the vacuum shroud of the cryostat. The opening of the inner tube toward the CsI window is surrounded by four nozzles through which Ar is directed to the same window to ensure efficient mixing with the substance emanating from the heated tube. To deposit **I3C** the inner glass tube was resistively heated to 58.5 °C.

Photolysis of indole and **I3C** was effected with a 1 kW Ar plasma arc lamp through a 280 cutoff filter. Electronic absorption spectra were recorded on a Perkin-Elmer Lambda 9 spectrometer.

To generate radical cations, 1% of CH_2Cl_2, which acts as an efficient electron scavenger, was added to the host gas mixture. The sample was exposed to 90 min of X-irradiation from a tube with a tungsten target operated at 40 kV/40 mA. The following net processes are thought to occur

$$Ar + h\nu(X) \rightarrow Ar^{\cdot+} + e^- \quad (1)$$

$$CH_2Cl_2 + e^- \rightarrow CH_2Cl^{\cdot} + Cl^- \quad (2)$$

$$Ar^{\cdot+} + \mathbf{S} \rightarrow S^{\cdot+} + Ar\ (\mathbf{S} = \text{indole or } \mathbf{13C}) \quad (3)$$

Measurements in Ionic Liquid. Glassy samples of 1-butyl-3-methylimidazolium hexafluorophosphate/methylene chloride

mixture ($BMIM^+PF_6^-$:CH_2Cl_2, 1:1 v/v) were prepared by immersing room-temperature solutions in liquid nitrogen in special cuvettes with an optical path length of 0.5−3 mm. These cuvettes were then placed in a liquid nitrogen-cooled cryostat (Oxford Instruments) where any temperature between 77 and 300 K can be maintained by controlled heating. The optical absorption spectra were measured on a Cary 5 (Varian) spectrometer. The samples mounted in the cryostat were irradiated with 4 μs electron pulses from an ELU-6 linear accelerator. In the figures of this paper, difference spectra are presented (after — before irradiation) to allow a direct comparison with the spectra obtained in the pulse radiolysis experiments (see below).

We have shown previously that ionic liquids, many of which form stable transparent glasses at 77 K,[14] can be used for generating radical ions by radiolysis. Recently we found that the glass quality does not change upon mixing $BMIM^+PF_6^-$ with CH_2Cl_2, which has the advantage that it improves the solubility of many precursors (such as **I3C** or **DIM**) and leads to a higher yield of radical cations on radiolysis due to its ability to scavenge electrons by dissociative attachment.[11] In addition, the $^{\bullet}CH_2Cl$ radicals formed in reaction 2 above can react on annealing of the matrix with the oxygen which is very difficult to eliminate from the ionic liquid to form peroxyl radicals that can further react with radical cations by hydrogen atom abstraction or may even oxidize radicals.

$$CH_2Cl_2 + e^- \rightarrow {}^{\bullet}CH_2Cl + Cl^- \quad (4)$$

$$^{\bullet}CH_2Cl + O_2 \rightarrow CH_2ClO_2^{\bullet} \quad (5)$$

Pulse Radiolysis. Pulse radiolysis experiments were carried out with high energy (8 MeV) 17 ns electron pulses generated from an ELU-6 Linac. The dose absorbed per pulse was determined with N_2O saturated aqueous solution of KSCN (0.01 M), assuming $G((SCN)_2^{\bullet-}) = 6.2 \times 10^{-7}$ mol/J and $\varepsilon((SCN)_2^{\bullet-}) = 7600\ M^{-1}cm^{-1}$ (G represents radiation chemical yield and ε is molar absorption coefficient at 475 nm).[15] The dose delivered per pulse was in the 5−80 Gy range. Low dose pulses were used for the determination of the rate constants of the reactions observed. Details of the pulse radiolysis system are given elsewhere.[16]

In order to study the reaction of **I3C** with hydroxy radicals, the aqueous solutions were deoxygenated and then saturated with N_2O in order to convert e_{aq} into $^{\bullet}OH$ radicals (reaction 6, $k = 8.7 \cdot 10^9\ M^{-1}\ s^{-1}$).[17,18]

$$e_{aq} + N_2O \rightarrow {}^{\bullet}OH + OH^- + N_2 \quad (6)$$

$$\textbf{I3C} + {}^{\bullet}OH \rightarrow \text{products} \quad (7)$$

For one-electron oxidation in pulse radiolysis experiments, $^{\bullet}N_3$ radicals or dibromide radical anions $Br_2^{\bullet-}$ are often used. We found that the strong oxidant, $Br_2^{\bullet-}$ [$E°(Br_2^{\bullet-}/2Br^-) = 1.63$ V vs NHE] is less suitable for monitoring the oxidation process, as the $Br_2^{\bullet-}$ absorption band at 360 nm overlaps with product absorption bands, in contrast to $^{\bullet}N_3$, which is still sufficiently strong to oxidize the **I3C** [$E°$ ($N_3^{\bullet}/N_3^-$) = 1.33 V vs NHE] but does not absorb above 300 nm. $^{\bullet}N_3$ was generated by pulse radiolysis in aqueous solutions of NaN_3 saturated with N_2O to generate $^{\bullet}OH$ radicals that react with azide anions to form the oxidizing species (reaction 8).[17,18]

$$N_3^- + {}^{\bullet}OH \rightarrow {}^{\bullet}N_3 + OH^- \quad (8)$$

The pH of the solutions was adjusted with perchloric acid, sodium hydroxide, or with a phosphate buffer.

Kinetic analyses were done by the Levenberg−Marquardt algorithm. First-order rate constants were evaluated from plots of ΔA vs time. Bimolecular rate constants were determined from the slope of the linear plot of pseudofirst order rate constants for the build-up of transient product absorption vs concentration.

Quantum Chemical Calculations. The geometries of all species were optimized by the B3LYP density functional method[19,20] as implemented in the Gaussian 03 suite of programs,[21] using the 6-31G* basis set.

Excited state energies were calculated at the B3LYP/6-31G* geometries by the CASSCF/CASPT2 method[22] with the ANO-S basis set of Pierloot et al.[23] In the CASSCF calculations of radicals and radical cations of **I** and **I3C**, we used an active space comprising 9 π-electrons in 10 π-MOs, and we averaged over 8 or 9 roots of A″ symmetry. In the CASPT2 calculations we set the IPEA parameter to zero, but shifted virtual MOs by 0.1 h to remove intruder states.[24] All CASSCF/CASPT2 calculations were carried out with the MOLCAS 6.4 program system.[25] In cases where such calculations were not possible due to the size of the system (**DIM** and related species), we

SCHEME 1: The Formation of I3C and DIM in the Metabolism of Glucobrassin

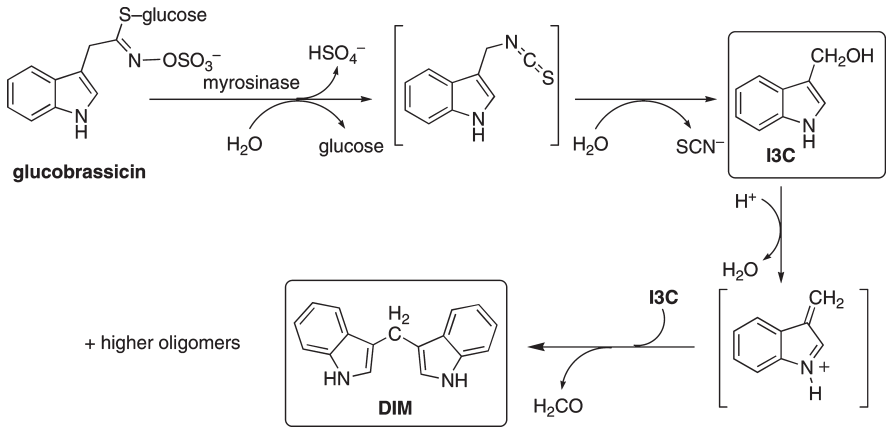

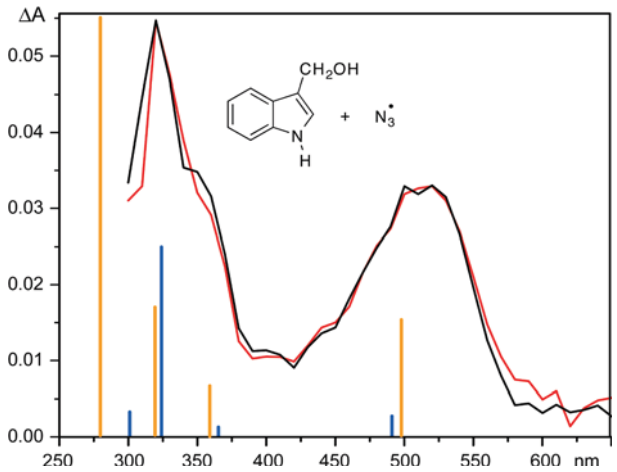

Figure 1. Transient spectra collected 8 μs after pulse radiolysis of **I3C** (0.08 mM) in an N_2O saturated aqueous solution containing 0.1 M NaN_3 at pH 7 (black line) and at pH 13 (0.1 M NaOH, red line). The blue bars denote electronic transitions predicted by the CASSCF/CASPT2 method for the radical obtained by deprotonation of **I3C**$^{\bullet+}$ at the CH_2 group, the orange bars for the radical obtained by deprotonation at the N-atom (cf. Scheme 2).

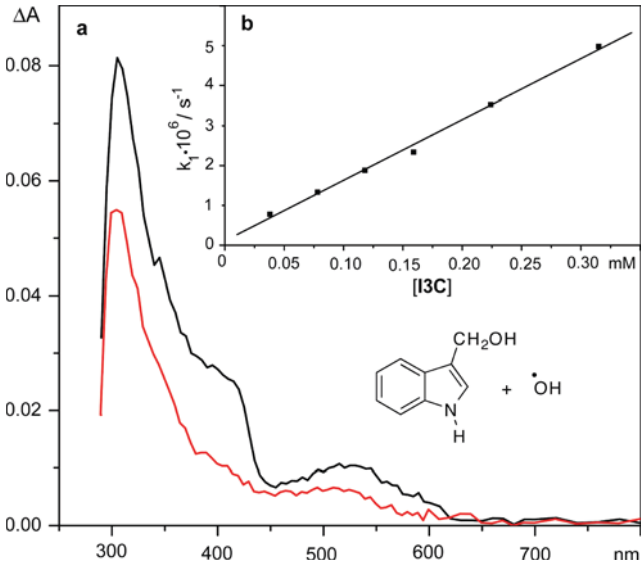

Figure 2. (a) Transient spectra obtained on pulse radiolysis of **I3C** (0.1 mM) in N_2O saturated aqueous solution at pH 7.4 (5 mM phosphate buffer). Spectra were collected 3 μs (black line) and 33 μs (red line) after the electron pulse. (b) dependence of the pseudofirst-order rate constant of product formation (λ_{obs} = 310 nm) on the concentration of **I3C**.

resorted to excited state calculation by density functional-based time-dependent response theory,[26] using the TD-B3LYP/6-31G* method.

The relative barriers for deprotonation of **I3C**$^{\bullet+}$ at the C- or the N-atom were calculated by embedding the molecule in a dielectric continuum with ϵ = 78, thus simulating the aqueous environment by SCRF calculations, and by transferring the proton to a molecule of ammonia (which corresponds to a slightly exothermic process under these conditions, water being too weak of a base to effect deprotonation of **I3C**$^{\bullet+}$under these conditions). In order to avoid difficulties in the cavity calculation, the migrating proton had to be fitted with its own sphere.

Results and Discussion

1. Reactivity of I3C toward Azidyl and Hydroxyl Radicals. Azidyl and hydroxyl radicals are strong one-electron oxidants that can be generated in situ by pulse radiolysis in aqueous solution (see above). Both have been used previously for oxidizing indole derivatives.[8−10] The transient spectra obtained on pulse radiolysis of aqueous **I3C** solutions in the presence of sodium azide at pH 7 and pH 13 are presented in Figure 1. The spectra formed 8 μs after the pulse under both conditions are identical, which proves that they cannot belong to **I3C**$^{\bullet+}$ (indole radical cations are known to persist only under acidic conditions[10] where **I3C** is, however, known to dimerize to **DIM**[1]). The spectra are characterized by absorption bands at 320 and 520 nm, which are similar to those found for indolyl radicals formed by deprotonation of indole radical cations.[9,10]

The reaction of **I3C** with hydroxyl radicals also results in the formation of some transient species. Figure 2a shows the spectra obtained on pulse irradiation of an N_2O saturated aqueous solution of **I3C** at pH 7.4 (conditions under which hydroxyl radicals are formed efficiently). Although the initial spectrum shows a weak band peaking at ca. 500 nm, accompanied by a stronger absorption above 300 nm, it is obvious that the reaction of **I3C** with •OH is not only a simple oxidation or dehydrogenation process, but that adducts are probably also formed. The build-up of product(s) absorbing at 310, 410, and 530 nm is observed to reach a maximum after 3 μs as determined at 310 nm. For kinetic analysis of the reaction the build-up of the absorbance at 310 nm was determined as a function of the concentration of **I3C** (see Figure 2b). From the slope of this plot a second order rate constant of 1.5 × 10^{10} M^{-1} s^{-1} was obtained, comparable to those for the reaction of other indole derivatives with •OH.[8] This value is close to the diffusion limit, indicating that **I3C** is a potent hydroxyl radical scavenger.

SCHEME 2: Possible Products of I3C$^{\bullet+}$ Deprotonation

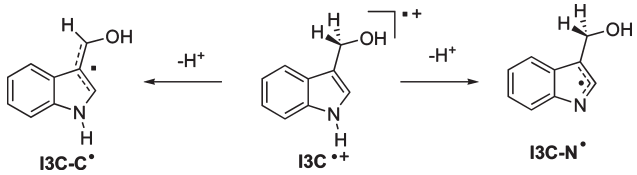

The above experiments indicate that **I3C** may form an indolyl radical when exposed to oxidants in vivo. However, in contrast to parent indole, **I3C** can undergo deprotonation at two sites, at the N-atom (leading to the radical **I3C**−**N**• in Scheme 2, or at the saturated C-atom, leading to **I3C**−**C**•.

In order to explore these two possibilities, and to assign the spectrum in Figure 1, we proceeded to model the two different deprotonation pathways by embedding **I3C**$^{\bullet+}$ and a molecule of ammonia, H-bonded once to the N−H and once to the CH_2-group, into a dielectric continuum with ϵ = 78. The results of this exercise are represented in Figure 3 which shows first that ammonia (and therefore any base) undergoes much stronger H-bonding to the N−H terminus of **I3C**$^{\bullet+}$ but that **I3C**−**C**• is slightly more stable than **I3C**−**N**• (if both are coordinated to the ammonium cation that results from proton transfer; for the free radicals in water the free energy difference increases to 8.7 kcal/mol). Starting from the two reactant complexes, the barriers for deprotonation are, however, very similar (1.22 and 1.43 kcal/mol for NH- and CH-deprotonation, respectively). Thus, if the coordination of the base to **I3C**$^{\bullet+}$ is an equilibrium process, deprotonation at the N-atom will prevail. Under kinetic control (e.g., if deprotonation occurs by water) a mixture of the two radicals will be expected to result.

On the other hand, to assign the observed spectra, we performed CASSCF/CASPT2 electronic structure calculations

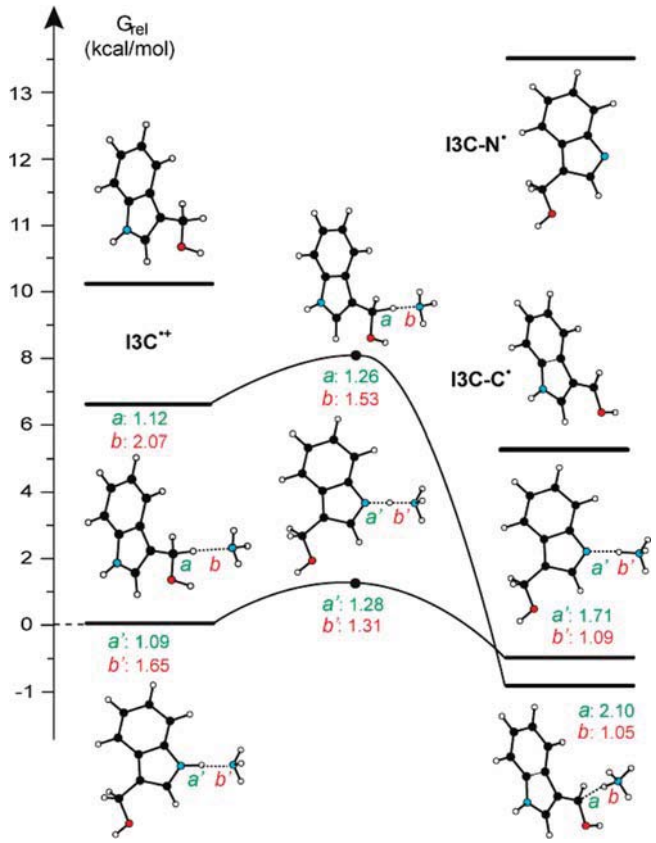

Figure 3. Thermochemistry and kinetics of the deprotonation of **I3C**$^{\bullet+}$ by NH_3 to form **I3C**$-$**N**$^{\bullet}$ and **I3C**$-$**C**$^{\bullet}$, respectively, in a dielectric continuum with $\epsilon = 78$ (free energies from B3LYP/6-31G* SCRF calculations in solution). The relative free energies of species unbound to NH_3 or NH_4^+ are shown as bars at the top.

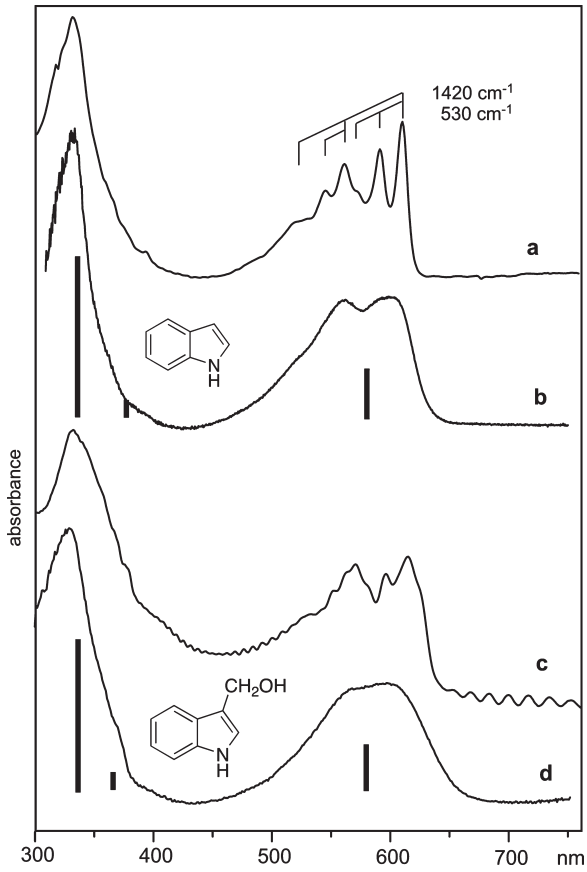

Figure 4. Electronic absorption spectra of of **I**$^{\bullet+}$ (a, b) and **I3C**$^{\bullet+}$ (c, d) in Ar at 10 K (a, c), and in $BMIM^+PF_6^-$ at 77 K (b, d). Bars indicate results from excited state CASSCF/CASPT2 calculations (cf. Table 1).

on **I3C**$-$**N**$^{\bullet}$ and **I3C**$-$**C**$^{\bullet}$, the results of which are indicated as blue and orange bars at the bottom of Figure 1 (a discussion of the electronic structure will follow in Section 2). As can be seen from these results, a weak band at ca. 500 nm and a strong band at ca. 320 nm (with a shoulder at ca. 360 nm) are predicted for both radicals, so the spectra shown in Figure 1 do not allow us to distinguish between the two species.

In conclusion of this section, it may very well be that in the pulse radiolysis experiments (as well as during in vivo oxidation of **I3C**), both radicals are formed simultaneously, if kinetic control of the deprotonation prevails. Under equilibrium conditions, **I3C**$-$**C**$^{\bullet}$ is expected to dominate.

To gain more insight into the electronic structure of the species involved in the above processes, we decided to investigate the title compounds, as well as parent indole, by matrix isolation spectroscopy.

2. Radicals Derived from Indole (I) and I3C. In Figure 4 the optical spectra obtained after X-radiolysis of indole (**I**) and **I3C**, respectively, in Ar at 10 K, and after pulse radiolysis of the same compounds in the ionic liquid at 77 K, are juxtaposed. The latter spectra show similar double humped bands peaking at ca. 600 nm, bands which reveal vibrational progressions of 1420 and 530 cm^{-1} in Ar (more clearly in the case of parent indole). We attribute these bands, as well as those peaking at ca. 330 nm, to the respective radical cations, because (a) these are the expected products under such conditions, (b) other indole derivatives have shown similar absorptions upon oxidation in solution,[8−10] and (c) CASSCF/CASPT2 calculations predict transitions and relative oscillator strengths in agreement with those shown in Figure 4.

The electronic structure of the indole radical cation is explained in Table 1 in terms of excitations involving the molecular orbitals shown in Figure 5. This analysis reveals that the observed visible band corresponds to the *second* excited state of the radical cation (all efforts to detect the very weak NIR transition to the first excited state failed), which is attained essentially by promotion of an electron from the third π-MO to the singly occupied MO (SOMO), π_5. The UV band seems to comprise a weak and a very strong transition, the latter corresponding mostly to excitation from the singly occupied MO (SOMO) to the LUMO, π_6*.

As the MOs π_3 and π_5 have very similar coefficients at the 3-position of indole (see Figure 5), their energy difference is not expected to change very much on substitution at this site. Indeed, CASSCF/CASPT2 predicts only a small shift in the excitation energy between the two radical cations (see stick spectra in Figure 4 and Table S1 in the Supporting Information), in accord with the previous observation that the radical cations of indole and tryptophan have very similar spectra.[9] In the case of the strong UV-transition a larger shift would be expected (cf. MOs π_5 and π_6), but that is not what the calculations predict.

With regard to the vibrational progressions of 1420 and 530 cm^{-1} observed in the Ar matrix spectra, CASSCF frequency calculations at the optimized structure of the second excited state of **I**$^{+\bullet}$ reveal indeed two normal modes, at 1387 and 557 cm^{-1}, that may be responsible for these vibrational progressions (see Figure 6). Both modes imply distortions such as they would be expected from the nodal properties of the MOs π_3 and π_5 between which an electron is promoted in the excitation. As CASSCF is not a very good method for predicting

TABLE 1: Electronic Structure of the Indole Radical Cation, $\mathbf{I}^{\bullet+}$, by CASSCF/CASPT2

state symmetry	CASSCF, eV	CASPT2, eV	CASPT2, nm	oscillator strength	CASSCF configuration[a]
1A″	(0)	(0)			80% ground config.
2A″	0.96	0.97	1284	9.21×10^{-5}	76% $\pi_4 \rightarrow \pi_5$
3A″	2.36	2.14	**580**	$\mathbf{4.75 \times 10^{-2}}$	**70% $\pi_3 \rightarrow \pi_5$**
4A″	3.54	3.29	377	6.00×10^{-3}	47% $\pi_2 \rightarrow \pi_5$; +11% $\pi_5 \rightarrow \pi_6$*
5A″	4.07	3.69	**336**	$\mathbf{1.55 \times 10^{-1}}$	**49% $\pi_5 \rightarrow \pi_6$***
6A″	5.08	4.49	276	1.96×10^{-2}	25% $\pi_5 \rightarrow \pi_7$*
7A″	5.45	4.85	255	1.60×10^{-1}	28% $\pi_4 \rightarrow \pi_6$*
8A″	5.71	4.99	248	5.10×10^{-3}	24% $\pi_1 \rightarrow \pi_5$

[a] In terms of the CASSCF MOs of $\mathbf{I}^{\bullet+}$ shown on the left-hand side of Figure 5.

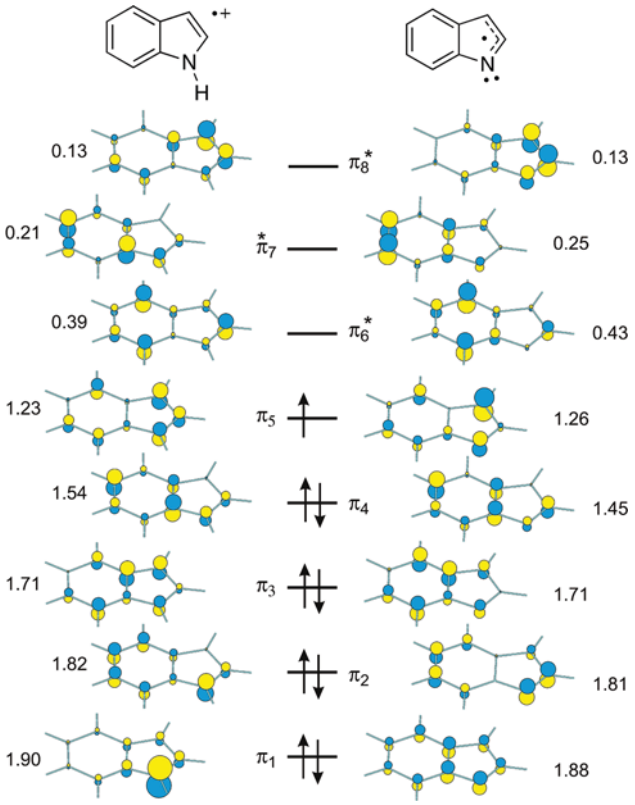

Figure 5. CASSCF molecular orbitals and fractional occupation numbers of $\mathbf{I}^{\bullet+}$ (left) and $\mathbf{I}^{\bullet}$ (right) involved in the electronic transitions of these species (cf. Tables 1 and 2).

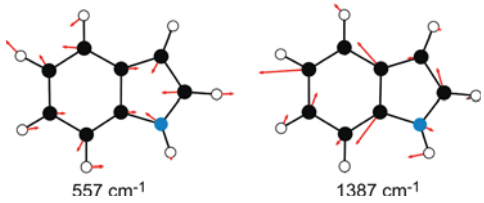

Figure 6. Vibrations causing the vibronic structure of the first absorption band of $\mathbf{I}^{\bullet+}$.

vibrational frequencies, the agreement between calculated and experimental frequencies must be regarded as quite satisfactory.

Somewhat surprisingly, both radical cations proved to be entirely photostable, that is, they showed no propensity for photodeprotonation, as it is sometimes observed in radical cations that can form stable radicals. Annealing experiments in ionic liquid glasses, which will be described in a separate paper, also did not yield any evidence for thermal deprotonation. Thus, we attempted to generate indolyl radicals by UV photolysis of **I** and **I3C** in Ar. The spectra that resulted from the experiments with these two compounds (see Figure 7) again show great similarities. As the only the (N-centered) 1-indolyl radical, $\mathbf{I}^{\bullet}$,

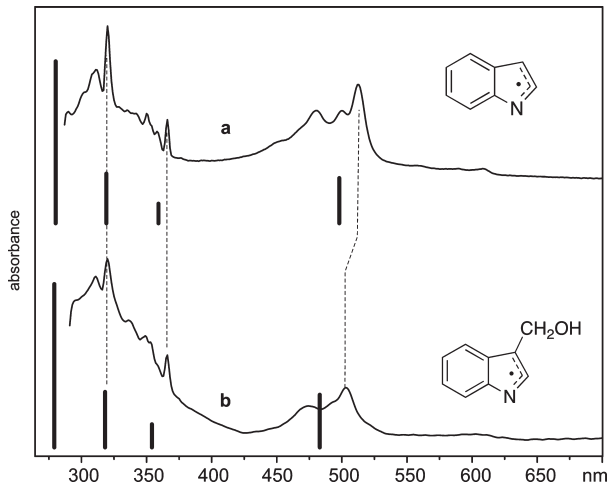

Figure 7. Spectra of $\mathbf{I}^{\bullet}$ (a) and $\mathbf{I3C}^{\bullet}$ (b). Bars indicate results from CASSCF/CASPT2 excited state calculations on the two radicals (cf. Table 2).

can be formed from indole, this indicates that a similar radical is also formed from **I3C**.

As in the case of $\mathbf{I}^{\bullet+}$, the visible band of $\mathbf{I}^{\bullet}$ and $\mathbf{I3C{-}N}^{\bullet}$ does not coincide with the first excited state, according to CASSCF/CASPT2 calculations (see Table 2; a similar Table for $\mathbf{I3C{-}N}^{\bullet}$ is in the Supporting Information, Table S2). In fact, the visible bands of $\mathbf{I}^{\bullet}$ and $\mathbf{I}^{\bullet+}$ look very similar, except that the frequencies of the vibrational progressions have changed sightly (in $\mathbf{I}^{\bullet}$ they are at 510 and 1250 cm^{-1}). Indeed, the π-MOs of the two species are very similar (see Figure 5), and the calculations show that the visible band corresponds to the same $\pi_3 \rightarrow \pi_5$ excitation, so the similarity of the 500 nm bands is not surprising. The higher excited states differ more between $\mathbf{I}^{\bullet}$ and $\mathbf{I}^{\bullet+}$. The calculations predict two transitions of medium intensity at ca. 360 and 320 nm, in good accord with the sharp band systems observed for $\mathbf{I}^{\bullet}$ and $\mathbf{I3C}^{\bullet}$ in this region. In fact, the calculations show that, although the visible absorption band is shifted by ca. 20 nm, the two UV bands occur at nearly the same energies in the two species, again in accord with experiment. Unfortunately, the strong absorptions of **I** and **I3C** block the region below 270 nm where both indolyl radicals are also predicted to have a strong band.

In view of what was said above, it is surprising that the same radical is exclusively formed from **I** and from **I3C**, as **I3C** has also the possibility to form a more stable C-centered radical, $\mathbf{I3C{-}C}^{\bullet}$, by losing a hydrogen atom from the CH_2 group. In an effort to prohibit formation of $\mathbf{I3C{-}N}^{\bullet}$ we tried to prepare the *N*-methyl derivative of **I3C**. However, this compound turned out to be surprisingly difficult to purify and to handle, so we had to seek another approach to the spectral characterization of $\mathbf{I3C{-}C}^{\bullet}$.

An alternative route to $\mathbf{I3C{-}C}^{\bullet}$ involves the radical anion of 3-formylindole, **3FI**, which can be generated by γ-irradiation

TABLE 2: Electronic Structure of the Indolyl Radical, I•, by CASSCF/CASPT2 Calculations[a]

state	CASSCF ΔE, eV	CASPT2 ΔE, eV	CASPT2, nm	oscillator strength	CASSCF configurations[b]
1A″	(0)	(0)			77% Ψ_0
2A″	1.23	1.14	1085	1.34×10^{-5}	68% $\pi_4 \rightarrow \pi_5$
3A″	2.81	2.49	498	1.53×10^{-2}	54% $\pi_3 \rightarrow \pi_5$
4A″	3.74	3.43	359	6.61×10^{-3}	38% $\pi_2 \rightarrow \pi_5$; +11% $\pi_5 \rightarrow \pi_6$*
5A″	4.26	3.89	319	1.68×10^{-2}	26% $\pi_5 \rightarrow \pi_6$*
6A″	5.87	4.74	280	5.48×10^{-2}	highly mixed

[a] With an active space of 9 electrons in 9 orbitals. [b] In terms of the CASSCF MOs of **I•** shown on the right-hand side of Figure 5.

SCHEME 3: Generation of I3C−C• from 3FI

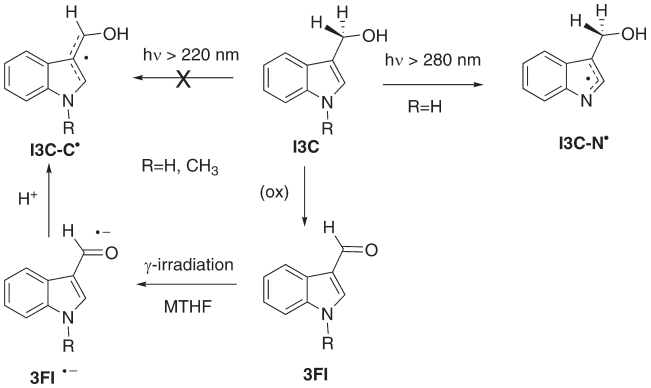

in MTHF or in an isopropanol glass,[27] where it can subsequently be protonated by the solvent to yield the targeted radical (Scheme 3). Figure 8 shows the spectra that were obtained in MTHF by this procedure, starting from **3FI** (its *N*-methyl derivative which, unlike N-methylated **I3C**, is a perfectly stable compound gives very similar spectra, see Supporting Information where the spectra of both compounds in isopropanol are also shown).

The spectrum obtained after radiolysis of **3FI** in MTHF shows a broad, intense band in the near IR, followed by a band peaking at ca. 680 nm and a steep rise below 400 nm. A part of the NIR band (which is also formed on radiolysis of pure MTHF and is therefore attributable to the solvated electron) can be readily photobleached. According to CASSCF/CASPT2 calculations (blue bars in Figure 8, for details see Supporting Information, Table S3), the remaining NIR band and the 680 nm peak may be assigned to the radical anion of **3FI**. On warming the matrix to 95 K, these two bands decay concomitantly while a new, sharper band emerges at ca. 545 nm. On further annealing this latter peak decays again and gives rise to several new bands between 350 and 530 nm (in the N-methyl derivative and in isopropanol, a band at 380 nm arises very prominently at this stage, see Figures S3−S5 in the Supporting Information). We have not been able to assign these bands to any plausible follow-up products, in contrast to that peaking at 545 nm which is in good accord with the weak transition predicted by CASSCF/CASPT2 for **I3C−C•** (cf. red bars in Figure 8, see also Figure 1 and Table S3 in the Supporting Information).

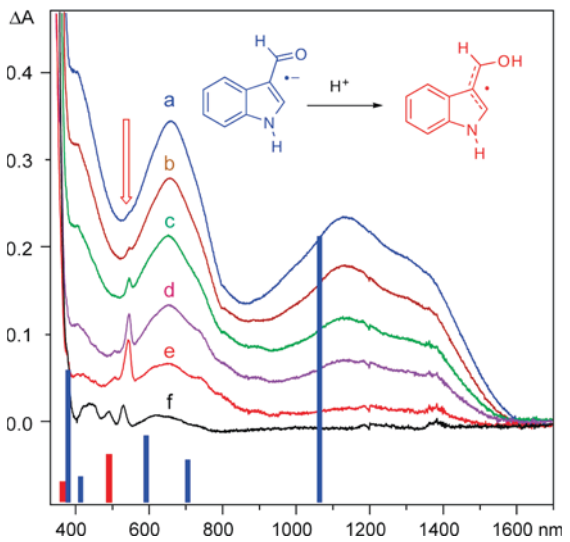

Figure 8. (a) Spectrum obtained on radiolysis of a 0.05 M solution of **3FI** in an MTHF glass at 77 K and subsequent bleaching of the solvated electron; this spectrum corresponds mostly to that of the **3FI** radical anion; (b−f) spectra obtained on subsequent stepwise annealing of the sample at 95 K, which leads to protonation of **3FI•−** and formation of **I3C−C•** (most prominently in spectrum e). The bars at the bottom represent electronic transitions and their relative intensities predicted by CASSCF/CASPT2 for **3FI•−** (blue) and for **I3C−C•** (red). For details of these calculations, see Tables S3 and S4 in the Supporting Information.

The observation of a band at 545 nm for **I3C−C•**, where **I3C−N•** also shows a band, and the lack of other distinct absorptions for this species confirms our hunch from the electronic structure calculations that the two allylic radicals that can be formed by loss of a hydrogen atom from **I3C** (or a proton from its radical cation) may be difficult to distinguish by optical spectroscopy. Thus, such spectra do not seem to form a reliable basis to decide which of the two radicals is formed in biological processes.

3. Radicals Derived from DIM. Our first investigations of **DIM** were again in the ionic liquid, $BMIM^+PF_6^-$, which had to be mixed with an equal part of CH_2Cl_2 to dissolve **DIM** to a concentration of 0.01 M. The spectrum obtained after radiolysis of the resulting glass at 77 K (Figure 9a) shows a double-humped band around 600 nm, similar to that observed with **I** and **I3C** under the same conditions (cf. Figure 3). Upon annealing at 135 K this band slowly decays and gives way to a new double-humped band peaking at ca. 490 nm. At the same time, a broad NIR band (not shown) and a sharper peak at 420 nm grow, but not in concert, so they must belong to different species. These bands decay again on further annealing at 200 K, while the 490 nm band continues to grow (not shown). Thus, the radical cation of **DIM**, which is presumably formed as a primary species on radiolysis, gives rise to at least three secondary products on annealing.

The last of these products can be easily identified as urorosein, the compound that stains urine pink under certain pathological conditions,[28] by comparison with an authentic sample, recorded in a 1 μM acidic ethanol solution (Figure 9e). Thus, it appears that, in the ionic liquid, **DIM+•** undergoes spontaneous loss of a hydrogen atom.

However, this process involves or is accompanied by the formation of transient species characterized by a weak absorption band around 420 nm, which initially grows, reaches a steady-state concentration, and eventually decays (in addition,

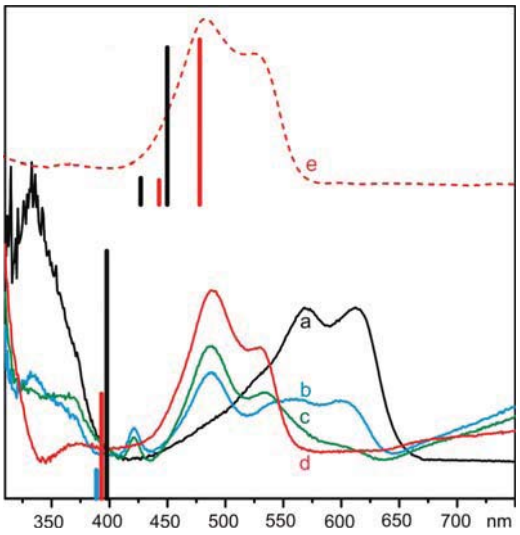

Figure 9. Spectrum obtained on radiolysis of **DIM** in a 1:1 mixture of $BMIM^+PF_6^-$ and CH_2Cl_2 at 77 K (a) and after annealing at 135 K for 30 min. (b), 145 K for 15 min. (c), 165 K for 15 min. (d); bars indicate results from TD-DFT calculations on the 3 conformations of **DIM-C**$^\bullet$; (e) Spectrum of **URS**$^+$ in acidic ethanol; black and red bars represent results from TD-DFT calculations on two conformers of urorosein, respectively (see text for discussion).

SCHEME 4: One Step vs Two Step (H^+/e^-) Hydrogen Atom Loss from DIM$^{\bullet+}$

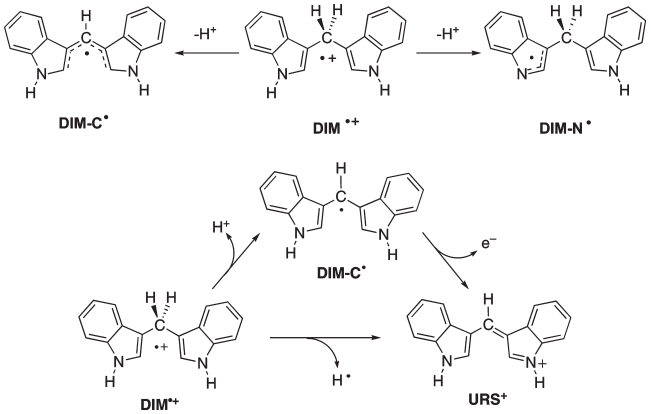

an NIR band rises concomitantly, but, as we will discuss in a separate paper, this has nothing to do with the formation of **URS**$^+$). The occurrence of this transient may suggest that urorosein is not formed in a single step, but may involve deprotonation to form **DIM-C**$^\bullet$ followed by ionization of this easily oxidizable radical (cf. Scheme 4).

Indeed, TD-DFT calculations predict that the strongest absorption of **DIM-C**$^\bullet$ (which differs slightly in the three conformers of that radical, cf. the discussion in the following section) occurs in the vicinity of the 420 nm peak of the observed transient. However, if that transient is indeed **DIM-C**$^\bullet$, it never appears in high concentration in the conversion of **DIM**$^{\bullet+}$ to **URS**$^+$.

We also investigated **DIM** in Ar matrices, but the results of this investigation, which have no direct bearing on the present study, will be communicated in a separate paper. We only wish to mention that, upon photolysis in Ar, **DIM** forms the N-centered radical, **DIM-N**$^\bullet$, in very small yield, but that no evidence for the formation of **DIM-C**$^\bullet$ can be obtained, either from **DIM** or from its radical cation.

4. Conformational Analysis of DIM-C$^\bullet$ **and URS**$^+$**.** A comparison of the spectra of **URS**$^+$ obtained by dissolving the

TABLE 3: Relative Free Energies of Different Conformations of URS$^+$ **and DIM-C**$^\bullet$

Conformer		dihedral angles d_1	dihedral angles d_2	ΔG (kcal/mol)
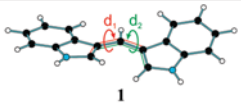 1	**DIM-C**$^\bullet$	11.4	-11.4	**(0)**[a]
	URS$^+$	16.9	-16.9	**(0)**[b]
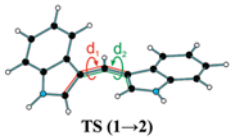 TS (1→2)	**URS**$^+$	-95.7	1.9	**16.7**[b]
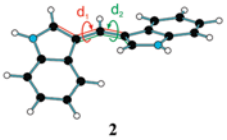 2	**DIM-C**$^\bullet$	156.2	13.8	**2.56**[a]
	URS$^+$	165.2	14.9	**0.40**[b]
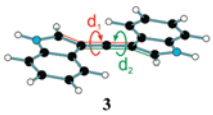 3	**DIM-C**$^\bullet$	158	-158	**4.90**[a]
	URS$^+$	162.4	-162.4	**1.98**[b]

[a] Calculations in gas phase; [b] SCRF calculations in ethanol.

authentic compound in acidic ethanol, and from **DIM**$^{\bullet+}$ in the ionic liquid, shows that the relative intensities of the two bands at 490 and 530 nm differ. This suggests that **URS**$^+$ can exist in different conformations, the proportions of which may change under varying conditions. B3LYP/6-31G* calculations (SCRF in ethanol for **URS**$^+$) showed that **URS**$^+$, as well as the closely related **DIM-C**$^\bullet$, indeed occurs as three stable conformers, the most stable of which has both NH groups facing away from the central C−H bond in a symmetric way (**1**) followed by one where the two indole rings are not far from being perpendicular to each other (**2**) for both species (see Table 3). A third conformer of C_2 symmetry, where the two N−H bond face the same way as the central C−H bond, lies about 2 kcal/mol higher in free energy in **URS**$^+$.

A variable temperature ^{1}H NMR spectroscopic study (see Figure S2 in the Supporting Information) indicated that at −60 °C two conformers of **URS**$^+$ are present in a ratio of ca. 6:1, where the predominant one has C_2 symmetry and the minor one has no symmetry. The calculated relative free energies of the three conformers of **URS**$^+$ (in EtOH as a continuum solvent) suggest that **1** is the dominant and that **2** is the minor species observed at −60 °C. In fact, the observed 6:1 ratio translates into a free energy difference between the two observed species of 0.7 kcal/mol, in good accord with the free energy difference of 0.4 kcal/mol between conformers **1** and **2** of **URS**$^+$calculated at the B3LYP/6-31G*/SCRF level.[29]

On warming the solution, all peaks begin to broaden until they coalesce near 0 °C and reemerge as averaged sharp signals at room temperature (see Figure S3 in the Supporting Information). This coalescence temperature, together with $\delta\nu = 400$ Hz, gives an estimate for the activation energy $\Delta G^{\ddagger} = 12.3$ kcal/mol for interconverting the two most stable conformers of **URS**$^+$. This is in rather poor accord with the theoretical prediction of $\Delta G^{\ddagger} = 16.7$ kcal/mol for the interconversion of conformers **1** and **2** of **URS**$^+$, but then B3LYP/6-31G* is not a level of theory of repute to yield accurate activation barriers.[30] Further warming leads to a shifting of these bands, which indicates that a third species, also with 2-fold symmetry, begins

to participate appreciably in the now rapidly established equilibrium, most probably conformer **3**, of $\mathbf{URS}^+$.

Table 3 lists also the relative free energies of conformers **1**−**3** of **DIM-C**$^\bullet$ (in the gas phase, as solvation is less important than in $\mathbf{URS}^+$). Here, conformer **1** is largely favored over **2** and **3**, but if **DIM-C**$^\bullet$ is formed from $\mathbf{DIM}^{+\bullet}$ then the conformational distribution may deviate strongly from the one that prevails at equilibrium.

TD-DFT calculations show that the different conformers of $\mathbf{URS}^+$ absorb at different wavelengths (in Figure 8e the absorptions of the two most stable confomers are indicated by black and red bars), thus confirming our assertion that the pair of bands observed around 500 nm in EtOH and in the ionic liquid is due to two conformers of $\mathbf{URS}^+$. In fact, these bands correspond to the first excited state of $\mathbf{URS}^+$, which is attained essentially by HOMO → LUMO electron promotion (higher excited states are due to promotion of the electron from lower lying doubly occupied MOs to LUMO).

Similar calculations predict that the three conformers of **DIM-C**$^\bullet$ absorb at very similar wavelengths, albeit with very different transition moments (see Figure 8). In this case, the ca. 400 nm band corresponds to the third excited state, which is attained essentially by HOMO → LUMO electron promotion (lower-lying states involve excitation of electron from doubly occupied MOs to the SOMO, but these give rise to transitions with very weak oscillator strength, see Supporting Information).

Conclusions

We have investigated the primary products obtained on oxidation of the glucobrassicin metabolites (and dietary supplements), **I3C** and **DIM**, in addition to that from parent **I**. The radical cations from all three compounds were generated by radiolysis in ionic liquid or Ar matrices at cryogenic temperature, identified by their electronic absorption spectra and characterized by excited state quantum chemical calculations.

We found that the radical cations of all three compounds are completely resistant to (photo-) deprotonation. The N-centered indolyl radicals of the three compounds can be formed by UV-photolyisis and deprotonation of the radical cations in aqueous solution, but no definite evidence was obtained for the formation of radicals that arise by H loss from the CH_2-groups of **I3C**, although calculations indicate that this radical should be more stable than the observed indolyl radical. In the case of **I3C**, the C-centered radicals could be generated by protonation of the radical anion of the corresponding aldehyde. In contrast to the radical cation of **I3C**, $\mathbf{DIM}^{\bullet+}$ seems to be more prone to deprotonation on the route to form the red urorosein cation, $\mathbf{URS}^+$, by sequential H^+/e^- loss.

Acknowledgment. This work was supported by grant from the Polish Ministry of Science and Higher Education (No. N205 003 32/0258). The Fribourg group acknowledges support by the Swiss National Science Foundation (project No. 20020-121747).

Supporting Information Available: Four additional Figures and the complete results of the CASSCF/CASPT2 calculations are contained in a pdf file, and a text-file contains the Cartesians and energies of all stationary points discussed in this study, and the results of TD-DFT calculations.

References and Notes

(1) http://lpi.oregonstate.edu/infocenter/phytochemicals/i3c/. Accessed June 2010.

(2) Agerbrink, N.; Olsen, C. E.; Sorensen, H. *J. Agric. Food Chem.* **1998**, *46*, 1563.

(3) Regal, K. A.; Laws, G. M.; Yuan, C.; Yost, G. S. *Chem. Res. Toxicol.* **2001**, *14*, 1014.

(4) Leete, E. *J. Am. Chem. Soc.* **1959**, *81*, 6023.

(5) See: http://www.diindolylmethane.org/ or http://www.dimfaq.com/index.htm. Accessed June 2010.

(6) See: http://www.cancer.gov/search/ResultsClinicalTrialsAdvanced.aspx? protocolsearchid=3883031. Accessed June 2010.

(7) Goyal, R. N.; Kumar, A.; Gupta, P. *J. Chem. Soc., Perkin Trans.* **2001**, *2*, 618.

(8) Shen, X.; Lind, J.; Merényi, G. *J. Phys. Chem.* **1987**, *81*, 4403.

(9) Solar, S.; Getoff, N.; Surdhar, P. S.; Armstrong, D. A.; Singh, A. *J. Phys. Chem.* **1991**, *95*, 3639.

(10) Jovanovic, S. V.; Steenken, S. *J. Phys. Chem.* **1992**, *96*, 6674.

(11) Czerwinska, M.; Sikora, A.; Szajerski, P.; Zielonka, J.; Adamus, J.; Marcinek, A.; Piech, K.; Bednarek, P.; Bally, T. *J. Org. Chem.* **2000**, *71*, 5312.

(12) Harley-Mason, J.; Bu'lock, J. D. *Biochem. J.* **1952**, *51*, 430.

(13) Bally, T. In *Reactive Intermediate Chemistry*; Moss, R. A., Platz, M. S., Jones, M., Eds.; Wiley & Sons: New York, 2004.

(14) Marcinek, A.; Zielonka, J.; Gębicki, J.; Gordon, C. M.; Dunkin, I. R. *J. Phys. Chem. A.* **2001**, *105*, 9305.

(15) Schuler, R. H.; Patterson, L. K.; Janata, E. *J. Phys. Chem.* **1980**, *84*, 2088.

(16) Karolczak, S.; Hodyr, K.; £ubis, R.; Kroh, J. *Radioanal. Nucl. Chem.* **1986**, *101*, 177.

(17) Neta, P.; Huie, R. E.; Ross, A. B. *J. Phys. Chem. Ref. Data* **1988**, *17*, 1027.

(18) Wardman, P. *J. Phys. Chem. Ref. Data* **1989**, *18*, 1637.

(19) Becke, A. D. *J. Chem. Phys.* **1993**, *98*, 5648.

(20) Lee, C.; Yang, W.; Parr, R. G. *Phys. Rev. B.* **1988**, *37*, 785.

(21) Frisch, M. J.; Trucks, G. W.; Schlegel, H. B.; Scuseria, G. E.; Robb, M. A.; Cheeseman, J. R.; Montgomery, J. A., Jr.; Vreven, T.; Kudin, K. N.; Burant, J. C.; Millam, J. M.; Iyengar, S. S.; Tomasi, J.; Barone, V.; Mennucci, B.; Cossi, M.; Scalmani, G.; Rega, N.; Petersson, G. A.; Nakatsuji, H.; Hada, M.; Ehara, M.; Toyota, K.; Fukuda, R.; Hasegawa, J.; Ishida, M.; Nakajima, T.; Honda, Y.; Kitao, O.; Nakai, H.; Klene, M.; Li, X.; Knox, J. E.; Hratchian, H. P.; Cross, J. B.; Bakken, V.; Adamo, C.; Jaramillo, J.; Gomperts, R.; Stratmann, R. E.; Yazyev, O.; Austin, A. J.; Cammi, R.; Pomelli, C.; Ochterski, J. W.; Ayala, P. Y.; Morokuma, K.; Voth, G. A.; Salvador, P.; Dannenberg, J. J.; Zakrzewski, V. G.; Dapprich, S.; Daniels, A. D.; Strain, M. C.; Farkas, O.; Malick, D. K.; Rabuck, A. D.; Raghavachari, K.; Foresman, J. B.; Ortiz, J. V.; Cui, Q.; Baboul, A. G.; Clifford, S.; Cioslowski, J.; Stefanov, B. B.; Liu, G.; Liashenko, A.; Piskorz, P.; Komaromi, I.; Martin, R. L.; Fox, D. J.; Keith, T.; Al-Laham, M. A.; Peng, C. Y.; Nanayakkara, A.; Challacombe, M.; Gill, P. M. W.; Johnson, B.; Chen, W.; Wong, M. W.; Gonzalez, C.; Pople, J. A. *Gaussian 03, Rev B.01*, Gaussian, Inc., Pittsburgh, 2003. During revision of the manuscript some additional calculations were done with Gaussian 09, Rev. A02 (see footnote 30).

(22) Andersson, K.; Roos, B. O. In *Modern Electronic Structure Theory*; World Scientific Publ. Co.: Singapore, 1995; Vol. 2, p 55.

(23) Pierloot, K.; Dumez, B.; Widmark, P.-O.; Roos, B. O. *Theor. Chim. Acta* **1995**, *90*, 87.

(24) Roos, B. O.; Andersson, K.; Fülscher, M. P.; Serrano-Andrés, L.; Pierloot, K.; Merchan, M.; Molina, V. *J. Mol. Struct (THEOCHEM)* **1996**, *388*, 257.

(25) Karlström, G.; Lindh, R.; Malmqvist, P. -Å.; Roos, B. O.; Ryde, U.; Veryazov, V.; Widmark, P.-O.; Cossi, M.; Schimmelpfennig, B.; Neogrady, P.; Seijo, L. *Comput. Mater. Sci.* **2003**, *28*, 222.

(26) Casida, M. E. In *Recent Advances in Density Functional Methods, Part I*; Chong, D. P., Ed.; World Scientific Publ. Co.: Singapore, 1995.

(27) Iwasaki, M.; Fukuya, M.; Fujii, S.; Muto, H. *J. Phys. Chem.* **1973**, *77*, 2739.

(28) Vinzenz, A. *Z. Physiol. Chem.* **1911**, *71*, 1.

(29) Bally, T., The calculation was done at room temperature, but if the entropy difference bewteen the conformers is assumed to be close to zero (which is supported by the gas-phase calculations), the free energy difference does not change much with temperature.

(30) At the suggestion of a referee we have recalculated this barrier at the B2PLYP level (with the 6-31G* basis set), accounting for solvation using the new model, implemented in the Gaussian 09 program, which makes the reaction field self-consistent with the MP2 density. At this level, the free energy of activation for conversion of **1** to **2** decreased to 14.5 kcal/mol, in much better accord with experiment. However, it should be noted that at this level, the relative free energies of the three conformers are also not the same: **2** is almost at the same free energy as **1**, whereas **3** lies only 0.95 kcal/mol higher. It is clear that even these calculations are fraught with so many approximations that it would be foolhardy to expect perfect agreement with experiment for a molecule the size of $\mathbf{URS}^+$.